

Maternal gut microbiota influences immune activation at the maternal-fetal interface affecting pregnancy outcome

Received: 14 May 2023

Accepted: 26 March 2025

Published online: 09 May 2025



Silvia Giugliano^{1,2}✉, Andrea Gatti^{2,3}, Martina Rusin^{1,2}, Tilo Schorn²,
Silvia Pimazzoni², Michela Calanni-Pileri^{1,2}, Valentina Fraccascia^{1,2},
Sara Carloni^{1,2} & Maria Rescigno^{1,2}✉

Preeclampsia is a leading cause of morbidity and mortality in pregnant women, affecting 5–8% of gestations worldwide. Its development is influenced by maternal immune abnormalities, metabolic disorders, and gut dysbiosis. In this study, we show that gut dysbiosis in pregnant C57BL/6J dams leads to increased fetal resorption, impaired placental development and altered vascularization. These adverse outcomes are associated with key pathological features of preeclampsia, including hypoxia, endoplasmic reticulum (ER) stress and reduction in uterine natural killer (NK) cell numbers. Furthermore, gut dysbiosis significantly perturbs placental carbohydrate metabolism, which impairs NK cell IFN- γ secretion. Notably, glucose supplementation restores placental NK cell function and reduces fetal resorption, suggesting that the observed impairment is reversible and dependent on a lower glycolytic rate. These findings highlight maternal gut microbiota as a key player in carbohydrate metabolism, with a pivotal role in modulating placental immunity and pregnancy outcome. The results provide valuable insights into potential metabolic biomarkers and suggest that targeting the gut microbiota may offer a strategy for preventing preeclampsia.

Preeclampsia is a leading cause of morbidity and mortality in pregnant women, affecting 5–8% of gestations worldwide¹. It is clinically manifested with hypertension, proteinuria, and multi-organ dysfunction, and is associated with pregnancy-related death, spontaneous abortion, and preterm delivery. Fetal complications include fetal growth restriction, preterm birth, and placental abruption, leading to significant developmental issues and even neonatal death². Despite this dramatic social and individual burden, preeclampsia can neither be reliably predicted nor effectively prevented³, with preterm delivery of the baby and placenta being the only cure³. The etiology of preeclampsia is complex and not completely understood.

The two-stage model of preeclampsia, as updated by Redman et al.⁴ proposes that preeclampsia develops in two distinct stages. The

first stage involves poor placentation, leading to placental malperfusion, hypoxia, and oxidative stress⁵. This stage is characterized by inadequate remodeling of the spiral arteries, restricting blood flow to the placenta⁶. The second stage is the maternal response to placental dysfunction, manifesting as the clinical symptoms of preeclampsia, including hypertension and proteinuria². This model emphasizes that the maternal syndrome is a consequence of factors released by the stressed placenta, interacting with maternal constitutional factors such as genetic predisposition and pre-existing conditions⁴, including abnormalities in maternal immunity, metabolic disorders, and gut microbial alterations^{7–9}.

Abnormalities in maternal immunity and gestational immune tolerance play a critical role in the pathogenesis of preeclampsia,

¹Department of Biomedical Sciences, Humanitas University, Pieve Emanuele, Milan 20072, Italy. ²IRCCS Humanitas Research Hospital, Rozzano, Milan 20089, Italy. ³Department of Medical Biotechnology and Translational Medicine, University of Milan, Milan 20133, Italy. ✉e-mail: silvia.giugliano@hunimed.eu; maria.rescigno@hunimed.eu

presumably during the first stage⁷. NK cells are the most abundant immune cell population at the maternal-fetal interface and play a major role in promoting placental vascular remodeling¹⁰. It has been shown that IFN- γ of uterine NK (uNK) cell origin is essential for spiral arterial remodeling in mouse pregnancy¹¹. In humans, first-time pregnancies are at a higher risk for miscarriages and preeclampsia¹². Studies on uteruses and placenta of women with repeated pregnancy have identified a subset of pregnancy-trained uNK cells able to produce higher levels of vascularization and angiogenic factors compared to first-time pregnancies¹³. These data suggest that uNK cells may provide memory to promote placental vascular remodeling during subsequent pregnancies.

Metabolic disorders such as obesity have also been postulated as putative factors related to preeclampsia. Obese women have an increased risk of developing preeclampsia that ranges between 10–15%⁸. The interconnection between the two diseases is still unknown, but clinical and experimental data suggest that obesity may affect placental function and perfusion through hyperlipidemia, hyperinsulinemia, or hyperleptinemia¹⁴.

The commensal microbial community in the human gastrointestinal tract plays crucial roles in both immune and metabolic homeostasis in normal pregnancy^{15,16}. Chen et al., have determined that patients with preeclampsia have disrupted microbiota composition, which contributes to disease pathogenesis⁹. Furthermore, increasing evidence has suggested that gut microbial metabolites could promote the onset of preeclampsia by directly inducing elevation in blood pressure¹⁷, modulation of the immune system, and alteration of blood vessel functions^{18,19}.

Considering the multifactorial nature of preeclampsia and the knowledge that altering the gut microbiome not only affects

inflammatory responses but also contributes to metabolic disorders and obesity²⁰. In this study we aimed to define how changes in the maternal gut microbiota could affect pregnancy outcome. We show that gut dysbiosis alters host metabolism predisposing to placental NK cell dysfunction and impaired placental vascularization. Specifically, we report that changes in gut microbiota composition during pregnancy significantly increased fetal resorption and altered placental vascular development. These changes positively correlated with the reduction of placental NK cell IFN- γ production induced by perturbation of placental carbohydrate metabolism.

Results

Gut microbiota changes alter fetal and placental development

Vancomycin is an antibiotic that is poorly absorbed in the intestine, hence, it is ideal to evaluate the effect of gut microbial alterations without inducing a systemic off-target effect²¹. To elucidate whether maternal gut microbiota impacts pregnancy outcome, we administered oral vancomycin (0.5 mg/ml) to C57BL/6J mice right after mating and continued treatment until sacrifice at embryonic day (ed) 12.5, ed14.5 and ed18.5 (Fig. 1a). Interestingly, vancomycin-treatment significantly increased fetal death and resorption at ed12.5 and ed14.5 leaving only a placental remnant, but not at ed18.5 (Fig. 1b, c). When addressing the impact of vancomycin-treatment on fetal weight, we observed a significant weight reduction at ed12.5 in the treatment group (Supplementary Fig. 1a). However, this trend reversed at ed14.5, likely due to a compensatory mechanism, as evidenced by the up-regulation of placental gene expression for amino acids and glucose transporters, including *Lat1*, *mTor*, *Glut1* and *Glut3*²², in the treatment group (Supplementary Fig. 1b). No significant differences in fetal weight were observed at ed18.5. To determine whether the differences

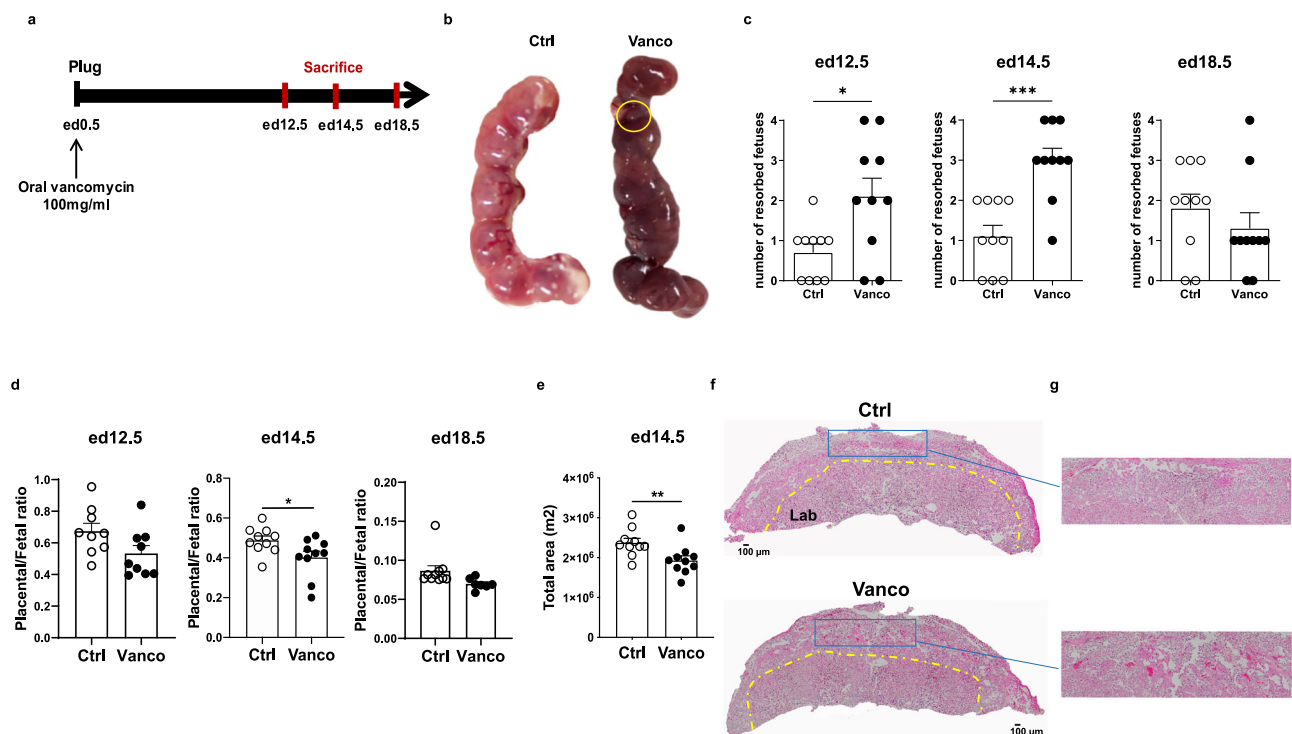


Fig. 1 | Antibiotic-induced microbiota alterations impact pregnancy outcome.

Schematic representation of the experimental plan (a). Vancomycin treatment (filled symbols) is associated with increased pregnancy loss and fetal resorption at embryonic day (ed) 12.5 ($p = 0.0259$) and ed14.5 ($p = 0.0003$) (b, c), significant reduction of placental/fetal ratio at ed14.5 ($p = 0.0115$, placental weight on fetal weight, d), reduction of the labyrinth area ($p = 0.0052$, e, f) and increased blood engorgement (g) compared to control pregnancies (open symbols) at ed14.5. Lines represent mean plus SEM, two-sided Mann Whitney test * $p < 0.05$, ** $p < 0.01$,

*** $p < 0.001$ (c–e). Magnification: 10X (f, g). ed: embryonic day; Lab: labyrinth. c includes 10 independent experiments. d represents 9 independent experiments for control and vancomycin-treated dams at ed12.5, 10 independent experiments for control and vancomycin-treated dams at ed14.5, and 10 independent experiments for control dams and 7 independent experiments for vancomycin-treated dams at ed18.5. In (e), 10 different placentas isolated from 5 experiments were measured. See also Supplementary Fig. 1. Source data are provided as a Source Data file.

observed at ed12.5 and 14.5 were linked to a loss of placental efficiency, we assessed the placental/fetal ratio, defined as the grams of fetus produced per gram of placenta²³. Notably, placental efficiency was significantly reduced in the vancomycin-treated group only at ed14.5 (Fig. 1d). We then evaluated whether the reduced placental/fetal ratio at ed14.5 was due to impaired placental development. We performed H&E staining on placental midline sections and analyzed the structure of the different placental layers. Of note, the labyrinth area, which is responsible for nutrients and gas exchange between the mother and the fetus, appeared to be significantly reduced in the vancomycin-treated dams (Fig. 1e, f). Increased blood engorgement in the outer zone was also observed, suggesting altered vascularization (Fig. 1g). These data indicate that vancomycin treatment elicits detrimental mechanisms able to impair placental development and impact normal fetal growth and development.

Gut dysbiosis alters placental vascularization and angiogenesis

To evaluate whether increased blood engorgement in vancomycin-treated dams was caused by altered placental vascularization, we stained midline placental sections with the erythroid marker Ter119 to distinguish between nucleated (fetal) and non-nucleated (maternal) erythrocytes, and the vascular endothelial marker CD31. As shown in Fig. 2a, b, CD31 signal was decreased in the treatment group revealing an altered pattern of expression compared to control dams. To better characterize whether altered vascularization also correlated with defects in angiogenesis we assessed the placental expression of α -smooth muscle actin (α -SMA) protein, a marker of spiral artery remodeling. Of note, α -SMA expression was higher in the treatment group compared to controls, suggesting that vancomycin-treatment might delay spiral artery remodeling, and impact the supply line to the fetus during gestation (Fig. 2c, d).

Having determined that vancomycin-treatment impacts placental vascularization and angiogenesis, we evaluated whether it could increase placental hypoxia. Elevated hypoxia in the human placenta has been linked to the disruption of placental and fetal development, contributing to neonatal impairments²⁴. As depicted in Fig. 2e, f, vancomycin administration significantly increased hypoxia-inducible factor-1 α (Hif-1 α), a protein stabilized under low-oxygen conditions. Placental hypoxia was further verified using Hypoxiprobe and assessing Hif-1 α target genes expression by RT-PCR. Increased hypoxic conditions in treated dams were confirmed by an upsurge in Hypoxiprobe signal in the placental junctional zone and labyrinth area (Fig. 2g–j), and in the expression of *Hif-1 α* and the Hif-1 α target genes, including *Inos* and *Glut3*, at the mRNA level (Fig. 2k and Supplementary Fig. 1b)²⁵. Chronic hypoxia induces ER stress in human placental trophoblasts. Therefore, we tested the expression of heat shock protein family chaperone binding immunoglobulin protein (BiP), an ER stressor sensor²⁶, in the placentas of treated and untreated dams. As shown in Supplementary Fig. 2, BiP expression was significantly up-regulated in vancomycin-treated dams compared to controls at ed14.5. These data indicate that vancomycin-treatment alters placental angiogenesis and vascularization, leading to reduced blood vessel maturation, hypoxia, and ER stress.

Gut dysbiosis impact placental vascularization via uNK cells

The fetal-maternal immune system plays a major role in pregnancy outcome²⁷. In particular, uterine (u)NK cells are known to be the major players in promoting placental vascularization during pregnancy through IFN- γ secretion²⁸. To assess whether vancomycin-treatment impacts on placental uNK cells which could then affect placental vascularization, we isolated placental immune cells across all three time points and evaluated IFN- γ production after 5 hours culture with PMA/ionomycin, see gating strategy in Supplementary Fig. 3a. Interestingly, we found that vancomycin-treatment decreased the percentage of IFN- γ positive placental NK cells and reduced their NKG2D

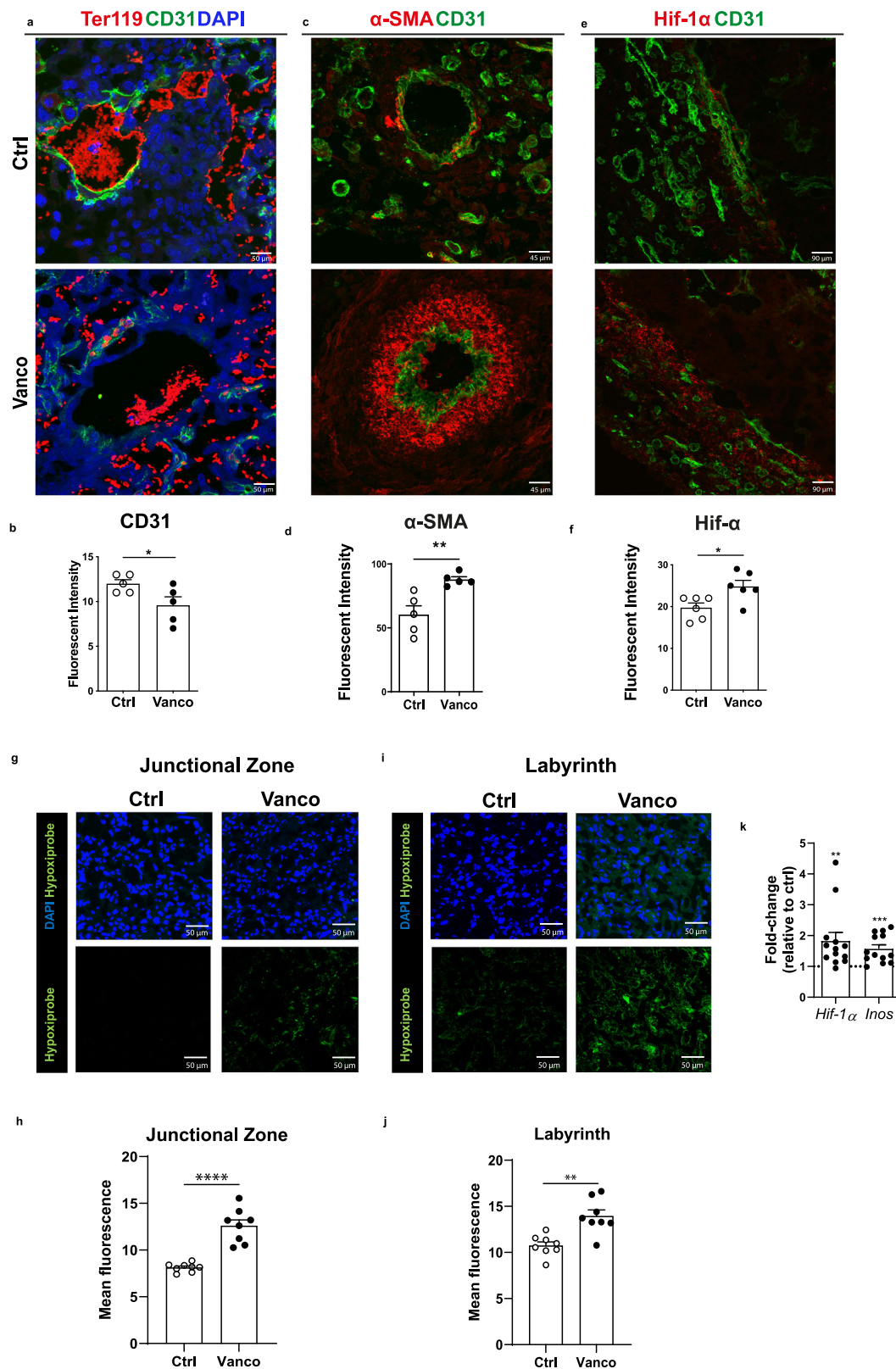
expression, while increasing the number of TNF positive NK cells at ed 14.5 (Fig. 3a, b). At ed12.5, we only observed a significant reduction in TNF production in the treatment group, while no differences were assessed at ed18.5 (Supplementary Fig. 3b, c). The total NK cell number was only slightly, and not significantly, reduced in the vancomycin-treated group at ed14.5. Significant reductions were instead observed in the treatment group when evaluating CD4⁺, CD8⁺ T cells and macrophages (M ϕ). (Supplementary Fig. 4). Consistent with the reduced placental efficiency, this suggests that the effects of vancomycin on immune cells are time-dependent, with the most pronounced changes occurring at ed14.5.

Gene expression studies have shown that *Dolichos biflorus* agglutinin (DBA) lectin⁺ uNK cells are the ones most involved in the expression of angiogenic factors²⁹. Having assessed that vancomycin-treatment alters placental NK cell activation and function, we evaluated whether delayed spiral artery remodeling could be due to a decrease in DBA⁺ uNK cells. As expected, we detected in vancomycin-treated dams a significant reduction of DBA⁺ uNK cells compared to control dams (Fig. 3c, d). Interestingly, this reduction positively correlated with significant lower placental expression of vascular endothelial growth factor-C (VEGF-C) (Fig. 3e, f). Of note, dysregulation of VEGF-C production by NK cell at the maternal-fetal interface causes poor angiogenesis and pregnancy complications³⁰. Interestingly, at the systemic level, VEGF-C levels were significantly increased in the serum of treated dams at ed12.5 and 14.5 (Supplementary Fig. 5a), aligning with previous studies showing increased serum VEGF levels in humans both before and during the onset of preeclampsia³¹. The Placental Growth Factor-2 (PlGF-2) was also up-regulated in the treatment group, though a significant difference was observed only at ed18.5. In contrast, serum levels of the Vascular Endothelial Growth Factor Receptor-1 (Flt-1) showed no substantial differences between treated and untreated dams (Supplementary Fig. 5b, c). Collectively, these findings suggest that vancomycin-treatment impairs placental vascularization by reducing DBA⁺ uNK cells, leading to decreased placental VEGF-C expression and delayed spiral artery remodeling. Dysregulated angiogenic factors, including increased systemic VEGF-C and altered PlGF-2 levels, may also contribute to placental dysfunction.

Gut maternal microbiota shifts linked to adverse pregnancy outcome

It is widely established that antibiotic treatment leads to changes in intestinal microbiota that are associated with various metabolic and immune diseases³². To understand the role of the vancomycin-modified microbiota on placental immune responses during gestation, we performed fecal microbiota transplantation (FMT) with stools from 7-day vancomycin-treated or untreated dams into pregnant dams. After mating, recipient pregnant dams underwent a three-day ampicillin treatment (1 mg/ml, from ed0.5 to ed3.5) before receiving the FMT via oral gavage (200 mg/ml, from ed3.5 to ed6.5) (Fig. 4a). Dams were then sacrificed at ed14.5 and immune cells isolated from the placental tissue. Interestingly, placental NK cells derived from dams transplanted with FMT from vancomycin-treated, but not from control dams, showed a significant reduction in IFN- γ and NKG2D expression, and increased TNF production (Fig. 4b). These FMT data nicely recapitulate the phenotype observed in our vancomycin-treatment model, exclude a vancomycin off-target effect, and suggest that changes in the maternal gut composition can modulate placental immune responses.

Our laboratory and others have previously shown that dysbiosis can alter intestinal epithelial and vascular permeability, leading to the translocation of bacteria and bacterial components to distant sites^{33,34}. To evaluate the level of dysbiosis and assess whether it may induce translocation of bacteria to the placenta and shift of NK cell phenotype, we performed microbiome analysis on feces and placentas of treated and untreated dams. Principle component analysis (PCA)



grouped together the fecal microbiota of vancomycin-treated dams at ed7.5, ed12.5, ed14.5, and 18.5 and separated them from the untreated samples, indicating an antibiotic-induced change in fecal microbiota composition. By contrast, no differences were detected in the two groups of placental samples at ed12.5, 14.5 and ed18.5 (Fig. 4c, Supplementary Figs. 6a and 7a). Similarly, when we analyzed the Shannon and Chao index, we could detect lower α -diversity in the fecal

microbiota of vancomycin-treated dams (ed7.5, ed12.5, ed14.5 and ed18.5), but not in the placental samples (ed12.5, ed14.5, and ed18.5) (Fig. 4d, Supplementary Figs. 6b and 7b). Vancomycin-treatment induced shifts in the taxonomic composition of the fecal samples, mainly causing an alteration in the *Firmicutes/Bacteroidota* ratio and an increase in *Proteobacteria*, while no major differences were detected in the placental-associated microbial DNA (Fig. 4e, f, Supplementary

Fig. 2 | Effects of antibiotic-induced microbiota alterations on placental vascularization and angiogenesis. Vancomycin treatment (filled symbols) is associated with a significant reduction of CD31 (green) signaling compared to controls (open symbols) at ed14.5 (a, b, $n = 5$ samples, $p = 0.0481$). On the contrary, α -SMA (red, c, d, $n = 5$ samples, $p = 0.0054$) and Hif-1 α (red, e, f, $n = 6$ samples, $p = 0.0194$) expression was increased in the treatment group (filled symbols) compared to controls (open symbols) at ed14.5. Lines represent mean plus SEM, two-sided Unpaired t test (b–f), $^*p < 0.05$. Magnification: 40X (A–C), 20X (e), TER119 (red), DAPI (blue). Multiple areas of the samples were measured, and placentas were harvested from 3 different experiments. Vancomycin treatment is associated with a significant increase of Hypoxiprobe signal (green and filled symbols) compared to

controls (open symbols) at ed14.5 in both the junctional zone (g, h, $n = 8$ samples, $p < 0.0001$) and labyrinth area (i, j, $n = 8$ samples, $p = 0.0010$). Magnification: 40X. Multiple areas of the samples were measured, DAPI (blue); placentas were harvested from 4 different experiments. Lines represent mean plus SEM, two-sided Unpaired t test (h–j), $^{**}p < 0.01$, $^{****}p < 0.0001$. Vancomycin-treatment induces significant up-regulation of *Hif-1 α* ($p = 0.0107$) and *Nos2* ($p = 0.0008$) genes in placental tissue at ed14.5 compared to controls ($n = 13$ samples, k). Gene up-regulation was assessed by real-time RT-PCR. Bars represent mean plus SEM, two-sided Wilcoxon signed-rank test, $^{***}p < 0.001$, $^{****}p < 0.0001$. Placentas were harvested from 3 different experiments. See also Supplementary Fig. 2. Source data are provided as a Source Data file.

Figs. 6c and 7c). Of note, we observed an increase of *Bacteroidota* in the gut of treated mice during gestation at ed14.5. These results nicely recapitulate human findings showing that at the third trimester of pregnancy preeclamptic women have significantly increased level of *Bacteroidota* compared to healthy controls³⁵. Furthermore, family and genera abundance comparison of gut microbiota composition showed increase of *Clostridiales* and depletion of *Lachnospiraceae* and *Ruminococcaceae* in the vancomycin-treated group across all three time points (Supplementary Fig. 6d, e, Supplementary Fig. 8). These changes are in accordance with Chen et al. showing a shift in the gut microbiota composition of preeclamptic patients recruited at the third trimester of pregnancy⁹.

To gain a comprehensive understanding of vancomycin-induced changes during pregnancy, we analyzed the microbiome in the vaginal fluid, uterus and saliva of treated and untreated pregnant dams at ed12.5, ed14.5 and ed18.5. At ed18.5, vancomycin-treated dams exhibited altered beta-diversity in the vaginal fluid, along with a non-significant trend toward reduced alpha diversity across all three time points. At the phylum level, vancomycin-treated dams showed a reduction in *Bacteroidota*, *Actinobacteriota*, and *Desulfobacterota*, alongside an increase in *Firmicutes*, *Verrucomicrobia*, and *Deferribacterota*. At the genus level, we observed a significant increase in *Akkermansia* and *Lactobacillus* in the vancomycin-treated, but only at ed18.5. (Supplementary Fig. 9a–d).

In the uterus, we detected a decreased Chao index at ed18.5, with no further differences observed in the Shannon index or beta diversity. At the phylum level, the uterine microbiota showed mostly an increase of *Proteobacteria* and a reduction of *Verrucomicrobia* and *Bacteroidota*. Notably, no statistically significant differences were observed at the genus level (Supplementary Fig. 9e–g).

For the oral microbiome, we anticipated greater differences between treated and untreated dams due to the direct exposure of the oral cavity to the antibiotic. While a trend towards reduced alpha diversity was observed, statistically significant differences were only identified in beta diversity across all three time points. At the phylum level, *Firmicutes* dominated the oral microbiome in treated animals, at the expenses of all the other phyla (Supplementary Fig. 10). At the genus level, we detected a significant reduction of *Streptococcus* across all three time points.

Overall, these data strongly suggest that while vancomycin-treatment induces changes in the maternal gut microbiome, it does not affect the placental microbiome. Significant differences were observed in vaginal fluid and uterus only at ed18.5. This finding suggests that the adverse pregnancy outcomes observed in our model are likely linked to microbial shifts at mucosal sites, primarily the gut, rather than in the placenta.

Impact of gut dysbiosis on the intestinal and placental metabolome

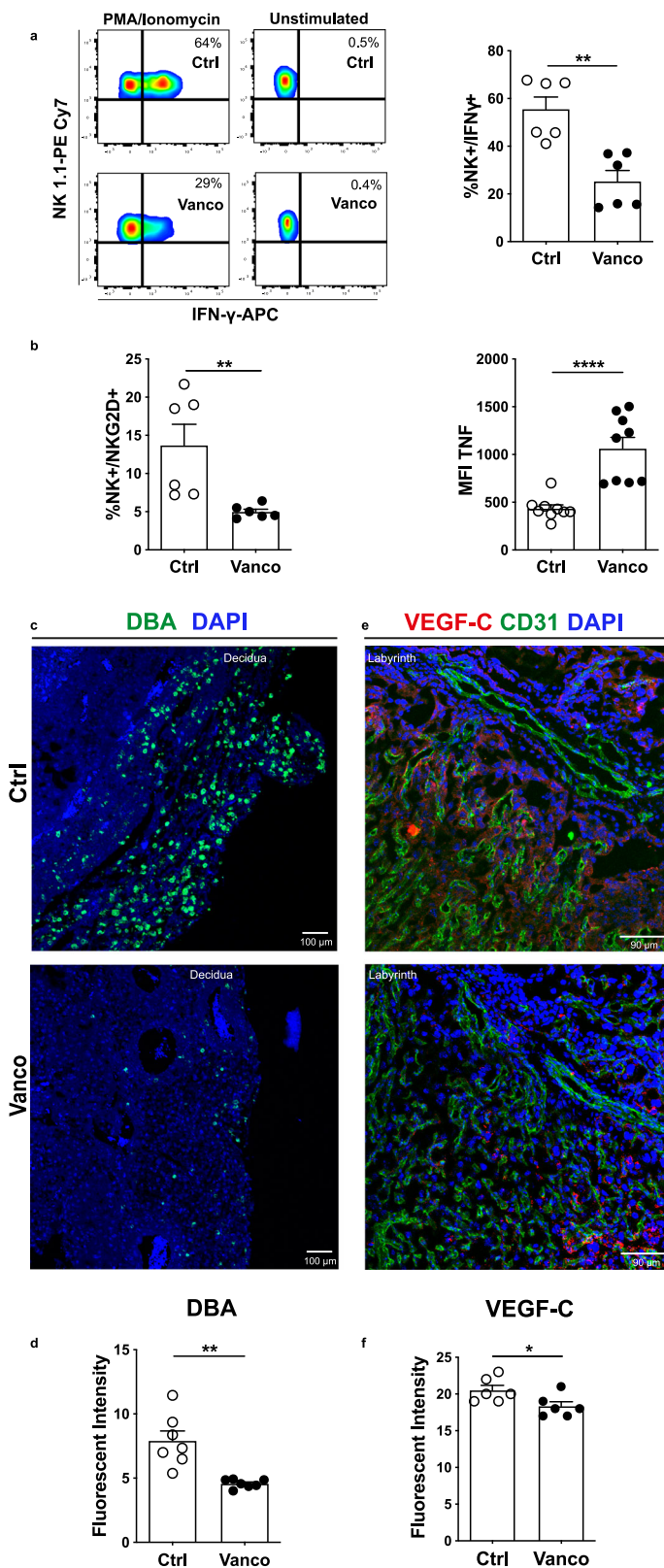
Modification of the gut- but not placental-microbiota in vancomycin-treated mice, ruled out the possibility that the alteration of NK cell immunity may be associated to a different placental microbiome induced by translocation of intestinal bacteria. As microbial metabolites have been shown to reach the placenta³⁶, we hypothesized that

alterations of NK cell activity may be due to a different metabolic output of the modified microbiota. We thus analyzed the fecal and placental metabolome of vancomycin-treated and untreated dams at ed14.5 when we observed major differences in placental development and immune activation.

PCA grouped together the fecal metabolome of vancomycin-treated dams at ed14.5 (light green dots) and separated them from the untreated samples (dark blue dots), indicating an antibiotic-induced change in metabolome composition as expected (Fig. 5a). Relative abundance analysis of metabolites with VIP score >1.5 in the PLS-DA model highlighted that vancomycin-treatment induced significant increase of propanoic acid, myo-inositol, ribonic acid, ribitol, valine, leucine, stearic acid and ribofuranose in the stools (Fig. 5b). To elucidate whether such increase was due to bacterial variations induced by vancomycin-treatment, we correlated bacterial shifts with metabolite abundance (Fig. 5c). Interestingly, *Bacteroidota* increase positively correlated with propanoic acid, myo-inositol, ribonic acid, and ribitol. *Firmicutes* decrease correlated with higher abundance of leucine, valine, and stearic acid. *Proteobacteria* increase positively correlated with myo-inositol and ribonic acid. Interestingly, glucose and rhamnose were not detected in the stools of vancomycin-treated dams. This is probably due to the elimination of anaerobic bacteria promoted by vancomycin-treatment³⁷, and to the fact that *Bacteroidota* and *Firmicutes* use hexoses and deoxy-sugars as main substrates for propanoic acid production³⁸. To confirm the impact of vancomycin-induced dysbiosis on hexoses availability, we analyzed the glucose level in the serum of FMT mice. In mice transplanted with feces from vancomycin-treated dams we detected a significant decrease of glucose compared to controls (Supplementary Fig. 11).

To identify biologically meaningful pathways significantly affected by vancomycin-treatment, we performed pathway and enrichment analysis based on Metaboanalyst 3.0. Using a p -value cut-off of 0.05 and an impact factor threshold >0 , we noticed that starch and sucrose metabolism (impact 0.04), galactose metabolism (impact 0.04), valine-leucine-isoleucine biosynthesis (impact 0.67) and inositol phosphate metabolism (impact 0.11) were the metabolic pathways most disturbed by vancomycin-treatment (Fig. 5d). These pathways are related to the carbohydrate metabolism and amino acid metabolism. Metabolites set enrichment overview confirmed these two metabolic groups to be the most disturbed by vancomycin-treatment (Fig. 5e). Of note, 9 out of 17 pathways significantly altered by vancomycin-treatment ($p < 0.05$) were affected by changes in glucose homeostasis. These results nicely suggest that vancomycin-induced dysbiosis elicits perturbations in maternal intestinal carbohydrate metabolism, which is known to play a pivotal role in pregnancy outcome and fetal development³⁹.

Having assessed the impact that gut dysbiosis has on intestinal metabolome and given the emerging role of metabolism in controlling NK cell function⁴⁰, we investigated whether vancomycin-treatment affected also the placental metabolome in pregnant dams. PCA grouped together the placental metabolome of vancomycin-treated dams at ed14.5 (light green dots) and separated them from the untreated samples (dark blue dots), indicating an antibiotic-induced



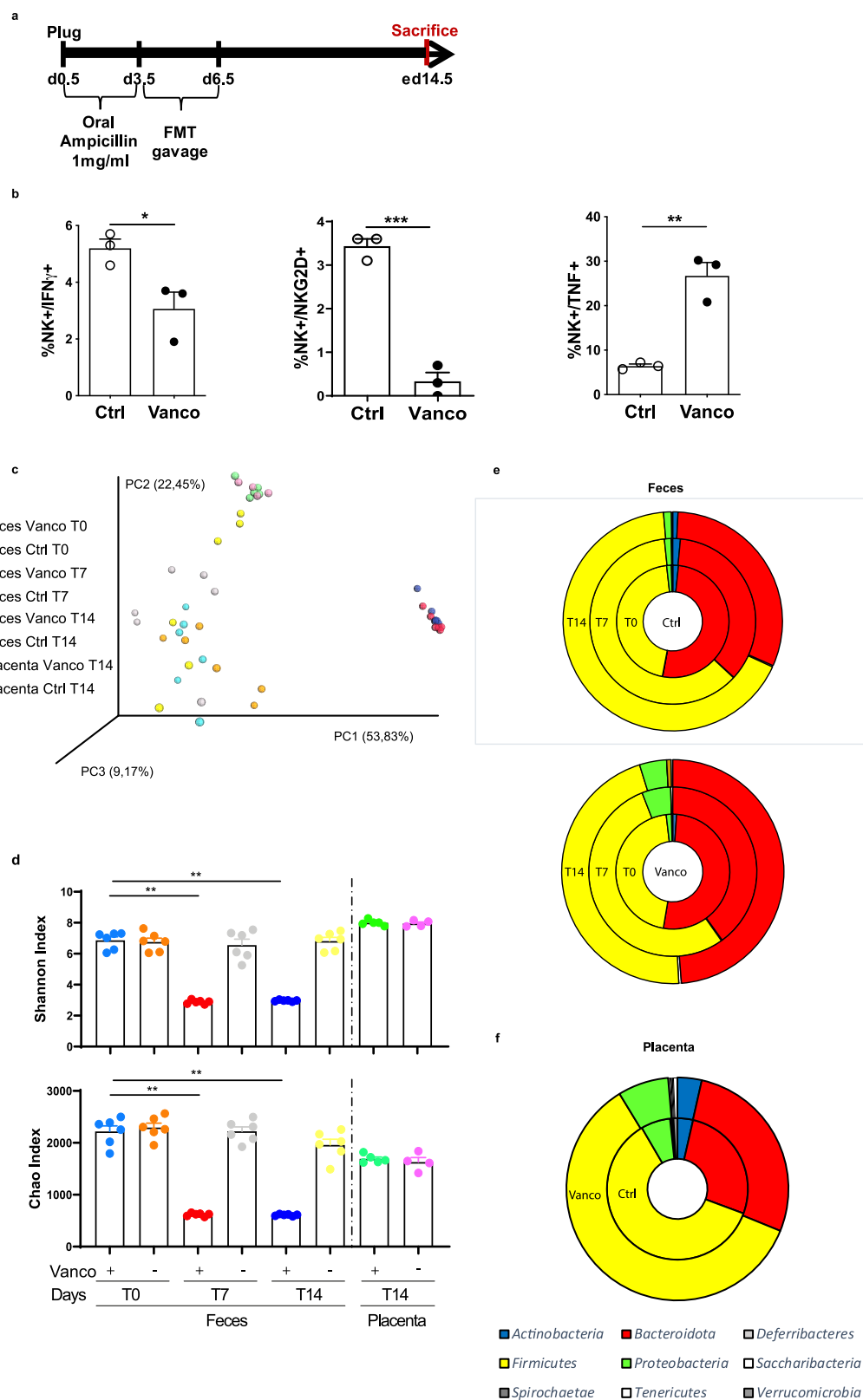
change in metabolome composition (Fig. 6a). Pathway analysis performed using a p -value cut-off of 0.05 and an impact factor threshold >0 , highlighted that carbohydrate, lipid, energy, and amino acid metabolism were the most perturbed pathways by vancomycin-treatment in the placenta (Fig. 6b). Of note, the metabolite set enrichment analysis assessed that also in the placenta, carbohydrate

Fig. 3 | Impact of antibiotic-induced microbiota alterations on placental immunity. Placental NK cells of vancomycin-treated dams (filled symbols) show significant less IFN- γ production (representative flow cytometry dot plot and statistical summary graph, **a**, $n = 6$ experiments, $p = 0.0022$), lower NKG2D expression ($n = 6$ experiments, $p = 0.0022$), and higher TNF ($n = 9$ experiments, $p < 0.0001$) secretion compared to control group (open symbols) at ed14.5 (**b**). Vancomycin treatment (filled symbols) is associated with significant decrease of DBA $^{+}$ uNK cell number in the decidua (green, **c**, **d**, $n = 7$ samples, $p = 0.0010$), and VEGF-C expression in the labyrinth area (red, **e**, **f**, $n = 6$ samples, $p = 0.0385$), compared to control pregnancies (open symbols) at ed14.5. Lines represent mean plus SEM, two-sided Mann Whitney t test (**a**, **b**), two-sided Unpaired t test (**d**–**f**), $^{*}p < 0.05$, $^{**}p < 0.01$, $^{***}p < 0.0001$. Magnification: 20X, DAPI (blue), CD31 (green, **c**–**e**). In **a** and **b** each measurement was taken from the placentas isolated from one single experiment, with all placentas from one dam combined into a single data point. In **d** and **f** different areas of the samples were analyzed; placentas were harvested from 3 different experiments. See also Supplementary Fig. 3, Supplementary Figs. 4 and 5. Source data are provided as a Source Data file.

metabolism and in particular galactose metabolism ($p = 0.018$) and the pentose phosphate pathway ($p = 0.03$), were the most disproportionately affected by vancomycin-treatment (Fig. 6c). Enrichment by pathway-associated metabolite sets was determined based on metabolites with a VIP > 1.5 (Supplementary Fig. 12). This result was particularly relevant to our study, since it has been shown that shifts between glucose and galactose metabolism slow down glycolysis and modulate IFN- γ secretion of human NK cells^{41,42}. To elucidate whether such shifts were occurring also in our model, we analyzed the relative abundance of glucose and galactose in the placentas of vancomycin-treated and control mice. Interestingly, placentas of vancomycin-treated dams showed higher relative abundance of galactose and a significant reduction of its metabolic breakdown product galactitol (Fig. 6d). No changes in placental glucose level were detected at ed14.5 (Supplementary Fig. 13) suggesting that a switch from glucose to galactose metabolism may occur in the placenta and might affect NK cell activity, presumably via the increase of galactose level.

To assess the effect of galactose on NK cell function we cultured placental NK cells isolated from untreated dams for 5 hours with PMA/ionomycin in the presence of glucose (20 mM), galactose (20 mM), or with two different glucose-galactose ratios, respectively 3:1 and 1:3. Interestingly, NK cells cultured with increasing concentrations of galactose showed significant reduction of IFN- γ production (Fig. 6e). Furthermore, to determine whether NK cell impairment could be restored by exposure to high glucose concentration, we cultured placental immune cells with PMA/ionomycin for 5 hours in the presence of glucose (50 mM). As shown in Supplementary Fig. 14a, high glucose concentration (filled squares) induced significant increase of IFN- γ production compared to glucose-free media (filled circles) in placental NK cells isolated from vancomycin-treated dams. Of note, placental NK cells isolated from untreated dams showed the same trend even though it was not significant (Supplementary Fig. 14b). Finally, to elucidate whether glucose administration could also play a role in vivo, we administered glucose orally at 30 g/kg for three days to vancomycin treated dams before sacrifice at ed14.5 (Fig. 6f). Of note, NK cells from glucose/vancomycin-treated dams showed a significant increase in IFN- γ secretion and a significant reduction of TNF production, restoring the phenotype. Significant reduction of fetal resorption in glucose/vancomycin-treated dams compared to the ones treated only with vancomycin was also observed (Fig. 6g). These data suggest that placental NK cell dysfunction in vancomycin-treated dams is reversible and is affected by a reduction in the glycolytic rate.

Collectively, these data highlight that vancomycin-driven microbiota changes lead to a shift in carbohydrate metabolism during pregnancy, which might play a pivotal role in altering placental immunity and pregnancy outcome.



Discussion

During pregnancy, the maternal body undergoes dramatic gut microbiome and metabolic changes to support fetal and placental growth⁴³. Factors such as antibiotics and stress can negatively affect gut microflora, leading to intestinal dysbiosis⁴⁴. Numerous studies have shown that changes in intestinal microbiota can adversely impact pregnancy outcomes and cause complications by disrupting maternal

adaptation^{45–47}. For instance, Chen et al. assessed that mice receiving fecal material from preeclamptic patients had elevated blood pressure even before pregnancy, indicating that gut dysbiosis induces hypertension independently of pregnancy⁹. Fecal mycobiota also differed in preeclamptic women in the third trimester compared to controls. Zou et al.⁴⁸ found that phylum *Ascomycota* was enriched in preeclamptic women, potentially impacting glycerophosphocholine levels, which

Fig. 4 | Impact of vancomycin-treatment on gut and placental microbiota during pregnancy. Schematic representation of FMT treatment performed in pregnant dams (a). Stools from vancomycin-treated mice (filled symbols) reduce IFN- γ ($p = 0.0329$), NKG2D ($p = 0.0004$) expression, and induce higher TNF ($p = 0.0025$) secretion in maternal NK cells compared to controls (open symbols) at ed14.5 ($n = 3$ experiments, b). Microbiome clustering based on unweighted Principal Coordinate Analysis (PCA) UniFrac metrics of fecal and placental microbiota derived from vancomycin-treated and untreated dams at T0 (feces ed0.5: light blue vancomycin, orange control), T7 (feces ed7.5: red vancomycin, gray control) and T14 (feces ed14.5: blue vancomycin, yellow control; placentas: green vancomycin, pink control, c). Graph showing microbial richness and evenness on the Shannon index (upper panel, T0 vs. T7 $p = 0.0022$, T0 vs. T14 $p = 0.0022$) and microbial

richness based on the Chao1 index (lower panel, d, T0 vs. T7 $p = 0.0022$, T0 vs. T14 $p = 0.0022$). The 16S analysis was performed on fecal samples from 6 control and 6 vancomycin-treated dams, as well as placental samples from 5 control and 4 vancomycin-treated dams. Pie charts showing the relative abundance of the most abundant Phyla present in the stool ($n = 6$, e) and placenta ($n = 6$, f) of treated and control groups (*Actinobacteria* = blue, *Bacteroidota* = red, *Deferribacteres* = light gray, *Firmicutes* = yellow, *Proteobacteria* = bright green, *Saccharibacteria* = dim green, *Spirochaetae* = dark grey, *Tenericutes* = brown, *Verrucomicrobia* = mid gray). Lines represent mean plus SEM, two-sided Unpaired t test (b), two-sided Mann Whitney t test (d), * $p < 0.05$, ** $p < 0.01$, *** $p < 0.001$. Each measurement was taken from a distinct experiment. See also Supplementary Figs. 6–10. Source data are provided as a Source Data file.

are related to preeclampsia. In this study, we show that maternal gut dysbiosis during pregnancy alters carbohydrate metabolism, blunting placental NK cell function and impacting pregnancy outcome.

Placental size, architecture, and metabolic interaction with the fetus are pivotal aspects for nutrient exchange and optimal fetal growth⁴⁹. We demonstrated that maternal gut dysbiosis, induced by vancomycin-treatment, significantly impact fetal growth and increases fetal resorption at embryonic day (ed) 14.5. This was confirmed by a reduction of the labyrinth area, essential for gas and nutrient exchange between the mother and the fetus. Blood engorgement within the labyrinth area suggested placental vascular impairment. Consistently, altered expression of CD31 and alpha smooth muscle actin (α -SMA) in the placental tissue of vancomycin-treated dams confirmed defective vascular development and spiral artery remodeling. Additionally, a higher hypoxic signal and increased expression of the hypoxia-inducible factor 1 alpha (Hif-1 α) gene were detected, with hypoxia further confirmed using Hypoxiprobe. In the human placenta, hypoxia is linked to pregnancy-associated disorders such as preeclampsia and fetal growth restriction⁵⁰. Furthermore, we detected increased expression of heat shock protein family chaperone binding immunoglobulin protein (BiP) in placentas from vancomycin-treated dams. BiP expression is a well-known signal of ER stress and is observed to increase in trophoblasts exposed to chronic hypoxia and in the placentas of preeclamptic patients²⁶.

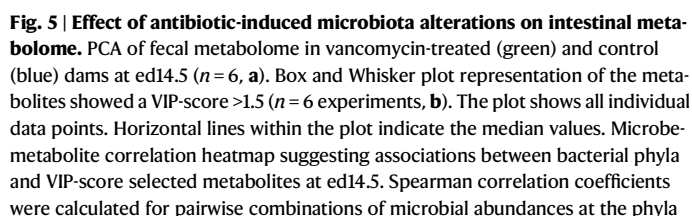
During pregnancy, uterine NK (uNK) cells constitute 70% of maternal lymphocyte fraction⁷. IFN- γ from uNK cells is essential for spiral artery remodeling in mouse pregnancy²⁸, and NK cell-deficient mice show defective vascular remodeling with thick vascular walls and retention of α -SMA¹⁰. In mice, two uNK cell populations are distinguished by their reactivity to *Dolichos biflorus* agglutinin (DBA). Gene expression studies showed that IFN- γ transcripts dominate in the DBA⁺ subset, whereas DBA⁺ uNK cells predominantly express transcripts for angiogenic factors²⁹. In our in vivo model, placental NK cells from vancomycin-treated dams showed significant reduced IFN- γ secretion and NKG2D expression compared to controls at ed14.5. Of note, placental NK cells of treated dams also showed increased TNF production, a key cytokine eliciting uNK cell-mediated fetal resorption⁵¹, and associated with maternal endothelial dysfunction⁵². Vancomycin-treatment also significantly reduced placental DBA⁺ NK cells and VEGF-C expression in placental tissue. VEGF-C production is a hallmark property of non-cytotoxic uNK cells⁵³, and it has been postulated that dysregulation in VEGF-C production at the maternal-fetal interface could signal poor angiogenesis and pregnancy complications such as intrauterine growth restriction and preeclampsia³⁰. This alteration of the angiogenic factors was also confirmed at the systemic level, with a significant increase of VEGF-C and PlGF-2 observed in vancomycin-treated dams compared to control³¹.

Chen et al., have shown that the gut microbiome of patients with preeclampsia is dysbiotic and contributes to disease progression⁹. To address whether maternal gut dysbiosis in our in vivo model promoted bacteria affecting placental NK cell function, we conducted fecal microbiota transplantation (FMT) in pregnant dams. We present data

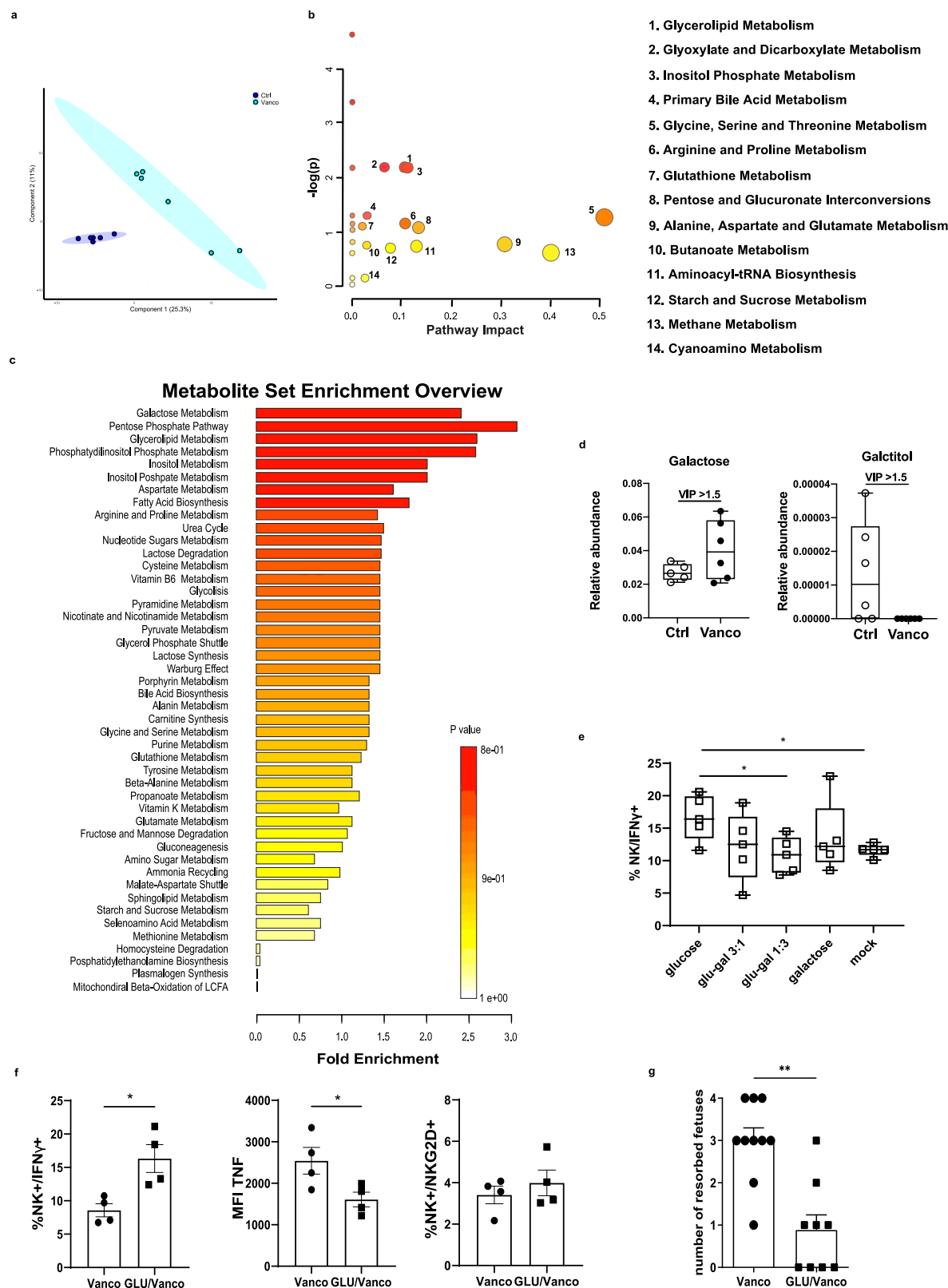
showing that stools from vancomycin-treated dams altered placental NK cell activation and function at ed14.5 by decreasing IFN- γ and NKG2D expression, while enhancing TNF production. These data fully recapitulated the phenotype obtained by vancomycin-treatment of pregnant dams.

Previous work has shown that preeclamptic women at the third trimester have a reduced *Firmicutes/Bacteroidota* ratio compared to healthy controls^{9,35}. To address whether this was also true in our mouse model, we analyzed the intestinal bacterial phyla at ed12.5, ed14.5 and ed18.5. Our analysis showed at ed14.5 a reduction in the *Firmicutes/Bacteroidota* ratio in vancomycin-treated dams. In the stools we also observed across all three time points, an increase in *Clostridiales* and a depletion of *Lachnospiraceae* and *Ruminococcaceae* similar to shifts seen in preeclamptic patients at the third trimester of pregnancy⁹. Interestingly, we could not detect significant changes in bacterial DNA in the placenta, and marginal differences in the vaginal fluid and uterus at ed14.5, suggesting that the microbial shifts induced by vancomycin in the gut are likely to be responsible for the observed phenotype. Gut microbiota has a significant role in maintaining energy harvest⁵⁴, immune homeostasis⁵⁵, and metabolism⁵⁶. Indeed, gut microbiota controls the metabolism of major nutrients like carbohydrate, amino acids, fatty acids, and vitamins. In this scenario, our data suggest that changes in the NK cell immune response might be due to metabolic alterations caused by intestinal dysbiosis, rather than the presence of bacteria in the placenta per se.

We have shown that vancomycin-treatment at ed14.5 dramatically altered the two major phyla in the intestinal microbiota, increasing *Bacteroidota* and decreasing *Firmicutes*. This change correlated with higher concentration of metabolites involved in glucose homeostasis at ed14.5, such as propanoic acid, valine and leucine in the treatment-group^{57–59}, and a drastic reduction of glucose and rhamnose, likely due to the elimination of anaerobic bacteria³⁷. These data align with Pugh et al.⁶⁰, who demonstrated that women with hypoglycemia had a higher likelihood of developing preeclampsia/eclampsia. Pathway and Metabolite Set Enrichment Analysis highlighted that vancomycin-induced dysbiosis in pregnant dams significantly altered carbohydrate and amino acid metabolism. Of note, similar metabolic perturbations were detected in the placenta, which also showed enrichment in the galactose metabolism. Galactose, metabolized by glycolysis through the Leloir pathway, converts to glucose-6-phosphate slowly, limiting glycolysis⁴². Previous work has shown that reduced glycolysis decreases NK cell IFN- γ secretion⁴¹. We demonstrated that vancomycin-driven dysbiosis interferes with placental development and vascularization by limiting metabolic fuel availability to placental NK cells. Exposure of placental NK cells to different glucose-galactose ratios, with increasing galactose concentrations over glucose, significantly reduced IFN- γ production. Furthermore, culturing placental defective NK cells isolated from treated dams in high glucose conditions restored their IFN- γ production, confirming a major role of carbohydrate metabolism in proper placental NK cell activity. The role of glucose availability in promoting correct placental NK cell function was also confirmed in vivo. Glucose was administered orally to vancomycin-treated dams



9



three days before sacrifice at ed14.5. Placental NK cells from vancomycin/glucose-treated dams showed a significant increase in IFN- γ production and a significant reduction in TNF secretion, effectively restoring the NK cell phenotype and reducing fetal resorption.

Collectively, these data provide insights into the interplay between gut microbiota, metabolism, and immune homeostasis, highlighting their crucial role in pregnancy outcome (Fig. 7). These

results have broader implications for identifying biomarkers and therapeutic targets for preventing pregnancy-related diseases like preeclampsia. They also suggest dietary supplementation could help restore the correct microbiota composition in pregnant mothers, while also emphasizing the potential risks of antibiotic treatments on placental and fetal development. Furthermore, these results underscore the importance of healthy eating to ensure adequate intake of

Fig. 6 | Effect of antibiotic-induced microbiota alterations on placental metabolome. PCA of placental metabolome in vancomycin-treated (green) and control (blue) dams at ed14.5 ($n = 6$, **a**). Pathway (**b**) and Metabolite Set Enrichment Analysis (**c**) of placental metabolites with a VIP score >1.5 at ed14.5. Global test algorithm was employed for both pathway impact and pathway enrichment analysis. Box and Whisker plot representation of galactose, and galactitol placental relative abundance at ed14.5 ($n = 6$ experiments, **d**). The plot shows all individual data points. Horizontal lines within the plot indicate the median values. Placental NK cells of control dams (ed14.5) significantly reduced IFN- γ production after 5 hours stimulation with PMA/ionomycin in media supplemented with a glucose:galactose ratio of 1:3 ($n = 5$ experiments, **e**, $p = 0.0209$). Placental NK cells of vancomycin-treated dams orally treated with 30 g/kg of glucose before sacrifice (ed14.5) show increased

IFN- γ ($p = 0.0151$) production and less TNF ($p = 0.0440$) production after 5 hours stimulation with PMA/ionomycin in media (filled squares) compared to vancomycin-treated dams (filled circles) (**f**). Two-sided Unpaired t test (**e**), the plot shows all individual data points. Horizontal lines within the plot indicate the median values. Lines represent mean plus SEM, two-sided Unpaired t test ($n = 4$ experiments, **f**), $*p < 0.05$, $****p < 0.0001$. Glucose administration to vancomycin-treated dams ($n = 9$, 30 g/kg per 3 days before sacrifice at ed14.5, squared filled symbols) decreases pregnancy loss compared to vancomycin treatment alone ($n = 10$ experiments, round filled symbols, g , $p = 0.0011$). Lines represent mean plus SEM, two-sided Mann and Whitney test, $**p < 0.01$. Each measurement was taken from a single experiment. See also Supplementary Figs. 12–14. Source data are provided as a Source Data file.

micro- and macronutrients, limit postprandial glucose excursions, and maintain glycemic control before and during pregnancy. This approach could reduce the risk of severe complications of pre-eclampsia, especially in high-risk women, such as those affected by type I diabetes and high BMI⁶¹.

Methods

Experimental model and animal details

Mice. This study was carried out in strict accordance with the recommendations in the Principles of Laboratory Animal Care (directive 86/609/EEC). The animal protocols (n. 998/16 and n. 320/2023-PR) were reviewed and approved by the Organismo Preposto al Benessere degli Animali (OPBA) and Italian Ministry of Health, Department of Veterinary Public Health, in compliance with national (D.L. N. 26, G.U. March 4, 2014) and international laws and policies (Directive 2010/63/EU). All mice used were on a C57BL/6 background. Female C57BL/6J OlaHsd mice (6 weeks old) were purchased from Envigo (Huntingdon, UK) and used for experiment one week after purchase. Male C57BL/6LY5.1 mice (6 weeks old) were obtained from Charles River laboratories (Wilmington, MA, USA) and used for mating. Both strains were housed 4–5 mice per cage at the Humanitas Research Hospital pathogen-free animal facility (SPF) in a temperature- and humidity-controlled environment ($22 \pm 2^\circ\text{C}$, 50–60% humidity) with free access to food (Cat#: DS811910G10R, Special Diets Services, Augy, France) and water and with 14 hours light/10 hours dark cycle. Following one week of acclimation the mating phase started until plug detection. Dams were then individually transferred in a new cage till sacrifice with Carbon dioxide (CO_2).

Antibiotic treatment

Dams were orally treated *ad libitum* with vancomycin (0.5 g/L, Vancomycin Hydrochloride Cat#: V-220-25, Goldbio, St Louis MO) from plug detection till sacrifice. Water bottles were changed every 5 days.

Fecal microbiota transfer

Feces from vancomycin-treated or control dams were collected, diluted in PBS (Cat#: ECB4053, Euroclone, Italy, 200 mg/ml), homogenized by vortexing and placed on a 70 μm filter centrifuged for 12 min at 3095 $\times g$ and stored at -80°C until use in PBS 80% glycerol (Cat#: G5516, Sigma, Merck, Germany). Before use, the diluted fecal solution was centrifuged at 17,949 $\times g$ for one minute and the pellet resuspended in 200 μL of PBS. Mice were orally treated with ampicillin (1 mg/ml) for 3 days, then gavaged three times with 200 μL of frozen diluted fecal contents belonging to the vancomycin-treated or control group. Mice were sacrificed at ed14.5 for placental immune cell isolation.

Method details

Measurement of cellular immune responses. Placentas were minced and digested with 10% collagenase D (Cat#: 1108886600, Sigma) in

Iscoe Modified Dulbecco Medium (Cat#: ECB2072L, Euroclone). Cells were dispersed into single cell suspensions with a 100 μm cell strainer and erythrocytes lysed (Cat#: F2360 COD 734-0004, Thermo Fisher Scientific, MA, USA). CD45 cells were purified by positive selection to greater than 90% using the CD45 Isolation kit (Cat#: 130-052-301, MACS Miltenyi Biotech, Germany).

Intracellular IFN- γ and TNF staining was performed after *in vitro* stimulation with PMA 50 ng/ml (Cat#: 79346-1M, Sigma) and ionomycin 500 ng/ml (Cat#: I0634-1MG, Sigma) for 5 hours, 10 mg/ml brefeldin A (Cat#: B6542-5MG, Sigma) were added after one-hour culture. Cells were stained with the following reagents and antibodies: Purified Rat Anti-Mouse CD16/CD32 (Cat#: 553141, BD Pharmingen, CA, USA, clone 2.4G2, dilution 1:50), CD45.1 (Cat#: 110716, 110706, 110714, Biolegend, CA, USA, 561872 BD Pharmingen, CA, clone A20, dilution 1:100), CD45.2 (Cat#: 553772, BD Pharmingen, 109808, 109814, Biolegend, 11045485, Thermo Fisher Scientific, clone 104, dilution 1:100), CD3 (Cat#: 152312, Biolegend, clone 500-A2, 100228, 100234, Biolegend, clone 17A2, 552774, 561826, BD Pharmingen, clone 145-2C11, dilution 1:100), NK1.1 (Cat#: 108714, Biolegend, clone PK136, dilution 1:100), NKG2D (Cat#: 562800, BD Horizon, clone CX5, dilution 1:100), CD4 (Cat#: 553730, BD, clone GK1.5, dilution 1:100), CD8 (Cat#: 557654, BD Pharmingen, clone 53-6.7, dilution 1:100), CD11c (Cat#: 560584, BD Pharmingen, clone HL3, dilution 1:100), CD11b (Cat#: 560455, BD Horizon, clone M1/70, dilution 1:100), F4/80 (Cat#: 123114, Biolegend, clone BM8, dilution 1:100), I-A/I-E Antibody (Cat#: 107628, Biolegend, clone:M5/114.15.2, dilution: 1:100), IFN- γ (Cat#: 505810, Biolegend, clone XMGL2, dilution 1:100), TNF (Cat#: 506306, 506304, Biolegend, clone MP6-XT22, dilution 1:100), and Fixable Viability Stain (Cat#: 65086314, 564406, BD, dilution: 1:1000). Data were collected on a BD FACSCanto II instrument (BD Biosciences) and analyzed using 390 DIVA software (BD Biosciences).

Immunohistochemistry

Mouse placental samples at ed14.5 were fixed in 4% PFA overnight, dehydrated through a series of increasing concentrations of ethanol, and embedded in paraffin. Sections (5- μm thick) were placed onto slides and subjected to H&E staining (Cat#: Ab245880, Abcam) on midline sections. Images were captured on VS120 Dot slide BX61 VS microscope (Olympus Corporation, Japan) at a 10X magnification. The labyrinth area was calculated using ImageJ software package [ImageJ [Internet] <https://imagej.nih.gov/ij/>].

Immunofluorescence and confocal microscopy

Mice were sacrificed at ed14.5, and placentas were harvested. The placentas were fixed overnight in paraformaldehyde 1%, L-Lysine pH 7.4 and NaIO4 (PLP buffer) for 24 hours. The next day, the placentas were transferred to a 20% sucrose solution for 24 hours. Finally, the placentas were embedded in optimum cutting temperature compound (OCT) and stored at -80°C until use. Subsequently, 12- μm thick frozen sections were cut with cryostat along the midsagittal plane. The following primary antibodies were used: Anti-mouse CD31 Armenian hamster antibody (Cat#: MAB1398Z, Merk Millipore, dilution 1:300,

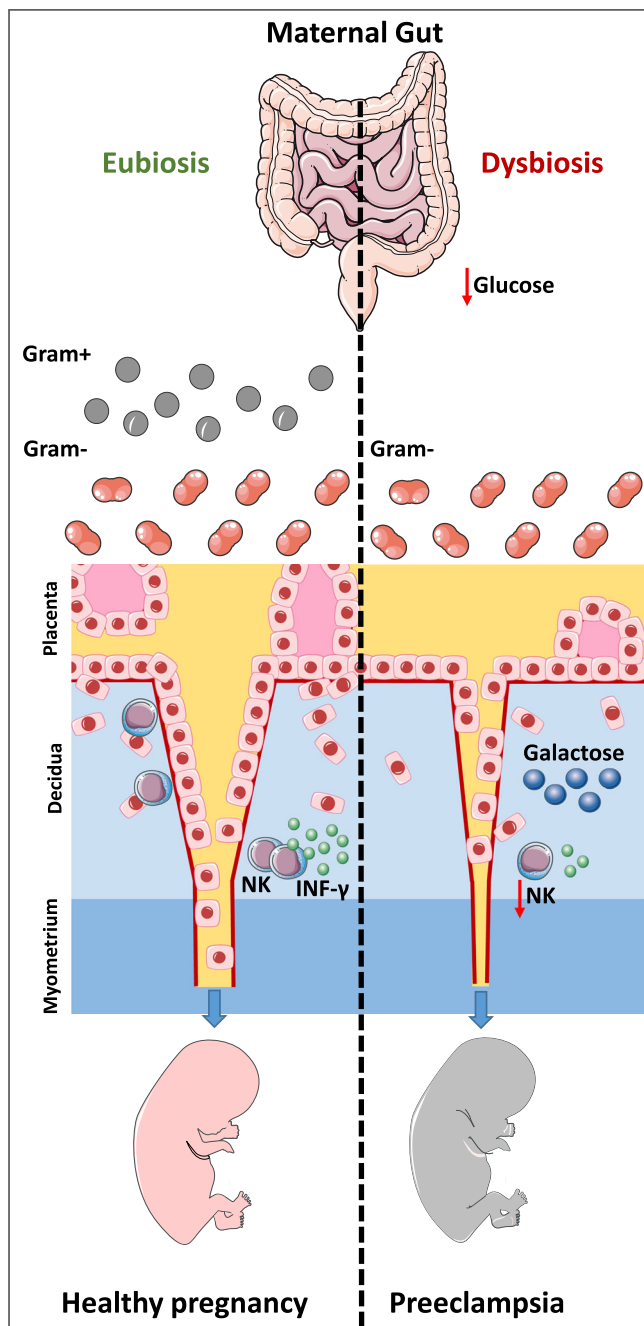


Fig. 7 | Impact of maternal gut dysbiosis on pregnancy outcome. Vancomycin-induced dysbiosis reduces intestinal glucose availability and alters placental carbohydrate metabolism causing a reduction of NK cells metabolic fuel availability. Such a shift directly impacts NK cell vascularization and angiogenic capacity, causing impairment of placental development and fetal resorption. This figure was generated using Servier Medical Art, provided by Servier, which is licensed under CC BY 4.0 (<https://creativecommons.org/licenses/by/4.0/>).

clone 2H8), anti-mouse TER-119 rat monoclonal antibody (Cat#: MAB1125, R&D System MN, USA, clone TER-119, dilution 1:1000.), anti-mouse HIF- α rabbit polyclonal antibody (Cat#: nb100-134, Novus Biologicals, CO, USA, dilution 1:100), anti-mouse VEGF-C rabbit polyclonal antibody (Cat#: ab135506, Abcam, dilution 1:100), anti-mouse α smooth muscle Actin (α -SMA) rabbit antibody polyclonal (Cat#: ab5694, Abcam, dilution 1:100), anti-mouse BiP rabbit monoclonal IgG (Cat#: 3177 T, Cell Signaling, MA, USA, dilution 1:200). The following conjugated, species-specific, cross-adsorbed detection antibodies were used: Alexa Fluor donkey anti rabbit 488 (Cat#: A21206, Thermo

Fischer Scientific, dilution 1:500), goat anti hamster cy3 (Cat#: 127165160, Jackson ImmunoResearch, PA, USA, dilution 1:500), donkey anti rabbit 555 (Cat#: A31572, Thermo Fischer Scientific, dilution 1:500), donkey anti rat 647 (Cat#: 712605153, Jackson ImmunoResearch, dilution 1:500). For uNK cell detection Biotinylated *Dolichos biflorus* agglutinin (DBA) (Cat#: B-1035, Vector Laboratories, CA, USA, dilution 1:200) and Streptavidin alexa flour 647 Conjugate (Cat#: S32357, Thermo Fisher Scientific, dilution 1:500) were used. Sections were then mounted with Vectashield mounting medium containing 4',6-diamidin-2-fenilindolo (DAPI) to counterstain the nuclei (Cat#: H-1200-10, Vector). Hypoxiprobe staining was performed following Hypoxiprobe Plus Kit, which includes anti-piminidazole antibody FITC-conjugated (Cat#: HP2-100kit, Hypoxiprobe inc., MA, USA, clone: 4.3.11.3, dilution 1:50). Tissue samples were analyzed with a Leica TCS SP8 Laser scanning confocal microscope (Leica, Germany). Emission filter bandwidths and sequential scanning acquisition were set up in order to avoid any possible spectral overlap between fluorophores. Images were acquired with a HC PL APO CS2 20X/0.75 dry objective and a HC PL APO CS2 40X/1.30 oil immersion objective (Leica). All the images were acquired as z-stack of the entire sections. ImageJ software package was used for image analysis and fluorescence quantification. To evaluate the contribution of marker expression the Mean Fluorescence Intensity was used.

RNA extraction and RT-PCR

Placental tissues were collected at ed14.5 and stored in RNeasy Lysis Buffer (Cat#: 76104, Qiagen, Valencia, CA, USA) until RNA isolation could be performed. Tissues were homogenized in Trizol, and total RNA was isolated following the manufacturer's instructions. RNA was further purified using RNeasy Midi Kit (Cat#: 75144, Qiagen), in conjunction with the RNeasy-Free DNase Set (Cat#: 75144, Qiagen), following the manufacturer's protocol to remove any contaminating DNA from the sample. Total RNA was then evaluated on a Nanodrop 1000 (Thermo Fisher Scientific) to confirm concentration and quality of the isolation. RNA quality was assessed using A260/A280 and A260/A230 absorbance values. Quantitative RT-PCR was performed using SYBR Green primers and master mix from Qiagen and run on a StepOnePlus quantitative PCR machine (Applied Biosystems, San Francisco, CA). Data were analyzed using the $\Delta\Delta C_T$ method. All primers used in the quantitative RT-PCR assays were purchased from Qiagen Cat#: 249900: *Hif-1 α* GeneGlobe ID: QT01039542, *Inos* GeneGlobe ID: QT01547980, *Lat1* (*SLC7A5*) GeneGlobe ID: QT01044932, *mTor* GeneGlobe ID: QT00118734, *Glut1* (*SLC2A1*) GeneGlobe ID: QT01044953, *Glut3* (*SLC2A3*): GeneGlobe ID QT00159691.

ELISAs

Flt-1 ELISA (Mouse VEGF Receptor 1/Flt1 ELISA Kit, Cat#: EMFLT1, Thermo Fisher Scientific), PlGF-2 ELISA (Mouse PlGF 2 (PGF) ELISA Kit, Cat#: EMPGF, Thermo Fisher Scientific), and VEGF-C ELISA Kit (Cat#: NBP2-78893, Novus Biologicals) were performed according to the manufacturer's instructions. All serum samples were collected at ed12.5, 14.5, and 18.5.

Microbiota Identification

Colonic feces (ed0.5, 7.5 and 14.5) and placental samples (ed14.5) from vancomycin-treated and controls dams were stored at -80°C until the DNA was extracted with G NOME DNA isolation kit (Cat#: 2010400, MP Biomedicals, Washington, DC, USA) following the previously described protocol⁶². Briefly, fecal pellets, were homogenized using 550 μl of Cell Suspension Solution from the G NOME DNA isolation Kit (Cat#: 2010400, MP Biomedicals). Subsequently, 50 μl of RNase Mix and 100 μl of Cell Lysis/Denaturing Solution from the same kit were added, followed by incubation at 55°C for 30 minutes. The samples were then treated with 25 μl of Protease Mix (G NOME DNA isolation Kit, Cat#: 2010400, MP Biomedicals) and incubated for an additional 2 hours at

55 °C. Bacterial cell disruption was achieved using 0.1 mm zirconia/silica beads (Cat#: #11070101z, BioSpec, Bartlesville, OK, USA) in a FastPrep®-24 homogenizer (MP Biomedicals). The lysates were collected, and the beads were rinsed three times with 400 µl of TENP buffer (50 mM Tris pH 8, 20 mM EDTA pH 8, 100 mM NaCl, 1% PVPP). The supernatants were combined with the initial lysate and precipitated using isopropanol. The resulting DNA pellet was dissolved in 400 µl of water and treated with 100 µl of Salt Out Mixture (G NOME DNA isolation Kit, Cat#: 2010400, MP Biomedicals) to eliminate impurities. DNA was precipitated with 100% ethanol, washed with 70% ethanol, air-dried, and finally reconstituted in water.

To avoid contamination during placental tissue isolation, uterine horns were carefully dissected, and fetuses (within the amniotic sacs attached to the placentas) were placed in separate Petri dishes. Placentas were then separated from the fetuses and frozen for further analysis.

Partial 16S rRNA gene sequences were amplified from extracted DNA using primer pair Probio_Uni (CCTACGGGRCAGCAG)/Probio_Rev (ATTACCGCGCTGCT), which target the V3 region of the 16S rRNA gene sequence⁶³. 16S rRNA gene sequencing was performed using a MiSeq (Illumina) at the DNA sequencing facility of GenProbio. Paired-end reads pairs were assembled to reconstruct the complete Probio_Uni/Probio_Rev amplicons. In order to calculate alpha diversity measures (Unifrac analysis), 16S rRNA Operational Taxonomic Units (OTUs) were defined at $\geq 99\%$ sequence homology using *ucrust*⁶⁴, and OTUs with less than 10 sequences were filtered. All reads were classified to the lowest possible taxonomic rank using QIIME⁶⁵ and a reference dataset from the SILVA database.

The bacterial profile at Phylum, family and genus was reported as a relative abundance. In detail, only taxa with relative abundance $> 0.5\%$ (or 1%) were shown. In order to associate *LpxC* gene locus to the Phyla, a list of bacterial cell envelope architecture published by Iain C. Sutcliffe⁶⁶ was used.

16S rRNA gene V3-V4 region from feces and placenta (ed12.5 and 18.5), saliva, vaginal, and uterus (ed12.5, 14.5 and 18.5) samples was amplified using QiaSeq 16S/ITS kit (Cat#: 333845, Qiagen) and the DNA sequencing was performed using Illumina MiSeq by Cogentech (www.cogentech.it). Following sequencing, the fastq files underwent QC filtering through *fastp* (v0.23.4) and *cutadapt* (v3.7), and reads with average quality score < 28 , with $0 + N$ base called and with mismatched primers were omitted. Custom scripts based on the QIIME2 software suite⁶⁵ were used to perform read denoising through DADA2 pipeline and obtain the ASV table, read classification through training of a Naïve-Bayes classifier using the extracted V3-V4 region from the SILVA 138 database (www.arb-silva.de). Subsequent analyses were performed on *Genus* taxonomic level count data. Alpha and Beta diversity analyses were carried out and coupled with circular taxa barplots considering each experimental timepoint of each region of interest individually. Downstream differential abundance analysis (DAA) was performed in R environment (v4.3.2, www.r-project.org), using the R package *Deseq2*⁶⁷. Taxa from count data were filtered based on the number of times they appear within the samples at each time point (threshold for filtering: $< 50\%$, meaning the feature had to appear in at least $\frac{1}{2}$ of the samples). Originated DAA PCA plot showing regularized log2-scaled sequence counts, heatmap displaying scaled counts, where the values are normalized by subtracting the mean taxa counts and dividing by their standard deviation of significantly different taxa, and barplot showing significant taxa and their respective shrunken log-fold change (LFC) for each timepoint and region are provided. DAA was performed with design vancomycin vs control condition, applied at each timepoint for each region of interest. The threshold for significance was set at adjusted *p*-value (Benjamini-Hochberg multiple test correction) < 0.05 , and for visualization purposes shrunken LFC > 0.5 or LFC < -0.5 . In addition, regularized log2-scaled counts PCA plots considering all time points and sample conditions are provided.

Metabolomics data analysis

Colonic feces (ed14.5) and placental samples (ed14.5) from vancomycin-treated and controls dams were stored at -80°C until processing. Metabolomics data analysis was performed on 24 samples, including fecal (ed14.5, control: $n = 6$; vancomycin-treated dams: $n = 6$) and placental samples (ed14.5, control: $n = 6$; vancomycin-treated dams: $n = 6$). The analysis utilized partial least square discriminant (PLS-DA)⁶⁸ on the normalized Internal Standard peak area⁶⁹. Classes separation was performed by PLS-DA regression performed using the *pls* function included in the R *pls* package⁷⁰. Using *Metaboanalyst3.0*, a weighted sum of squares from PLS was calculated as Variable Importance in Projection (VIP). Box&Whisker plots were used to represent the most relevant changes of metabolites between vancomycin-treated and control dams. Variations with a VIP score of at least 1.5 were considered relevant. Fecal metabolite abundances were tested for association to 16S levels using Spearman rank correlation. Pathway Impact and Metabolite Sets enrichment were performed using *Metaboanalyst3.0* (<http://www.metaboanalyst.ca>). For details on metabolome extraction, purification and derivatization, and metabolomics data analysis please refer to the Supplementary Method section.

Quantification and statistical analysis

Statistica analyses. The experiments were randomized, and the investigators were not blinded to allocation during experiments and outcome assessment. This study focuses on preeclampsia, a pregnancy-specific condition; therefore, sex was not considered in the study design or analysis. Data were analyzed using Prism software (GraphPad8, GraphPad9, GraphPad 10, San Diego, CA). Statistical details of experiments and the two-sided tests used to analyze experiments are described in the Figure Legends. Based on our laboratory experience, we initially estimated that to assess microbiological factors that could elicit further immunological, histological, and metabolomic differences in our mouse model, we would need at least $N = 6$ mice per group. This estimation was made with an effect size of 2, an alpha error of 0.05, and a power of 80%. According to the different data, statistical analysis between groups were analyzed using Wilcoxon's rank-sum test, Unpaired t test or nonparametric Mann-Whitney test. Correlation analysis was performed based on Spearman's rank test. A *p*-value of less than 0.05 is considered statistically significant.

Reporting summary

Further information on research design is available in the Nature Portfolio Reporting Summary linked to this article.

Data availability

The 16S data supporting the current study have been deposited to Zenodo public repository <https://doi.org/10.5281/zenodo.7848183>. The metabolomics data supporting this study are available in the MetaboLights repository with the study identifier MTBLS12316: <https://www.ebi.ac.uk/metabolights/MTBLS12316>. Further information and requests for resources and reagents should be directed to and will be fulfilled by the Corresponding Author, Maria Rescigno (maria.rescigno@hunimed.eu). All unique/stable reagents generated in this study are available from the Corresponding Author with a completed Materials Transfer Agreement. Source data are provided with this paper.

References

1. Abalos, E., Cuesta, C., Grosso, A. L., Chou, D. & Say, L. Global and regional estimates of preeclampsia and eclampsia: a systematic review. *Eur. J. Obstet. Gynecol. Reprod. Biol.* **170**, 1–7 (2013).
2. Brown, M. A. et al. Hypertensive disorders of pregnancy: ISSHP classification, diagnosis, and management recommendations for International Practice. *Hypertension* **72**, 24–43 (2018).

3. Roberts, J. M. et al. Hypertension in pregnancy. Report of the American College of Obstetricians and Gynecologists' Task Force on Hypertension in Pregnancy. *Obstet. Gynecol.* **122**, 1122–1131 (2013).
4. Redman, C. W. G., Staff, A. C. & Roberts, J. M. Syncytiotrophoblast stress in preeclampsia: the convergence point for multiple pathways. *Am. J. Obstet. Gynecol.* **226**, S907–S927 (2022).
5. Burton, G. J. Oxygen, the Janus gas; its effects on human placental development and function. *J. Anat.* **215**, 27–35 (2009).
6. Burton, G. J., Watson, A. L., Hempstock, J., Skepper, J. N. & Jauniaux, E. Uterine glands provide histiotrophic nutrition for the human fetus during the first trimester of pregnancy. *J. Clin. Endocrinol. Metab.* **87**, 2954–2959 (2002).
7. Erlebacher, A. Immunology of the maternal-fetal interface. *Annu. Rev. Immunol.* **31**, 387–411 (2013).
8. Catalano, P. M. Obesity, insulin resistance, and pregnancy outcome. *Reproduction* **140**, 365–371 (2010).
9. Chen, X. et al. Gut dysbiosis induces the development of preeclampsia through bacterial translocation. *Gut*, [gutjnl-2019-319101](https://doi.org/10.1136/gutjnl-2019-319101) <https://doi.org/10.1136/gutjnl-2019-319101> (2020).
10. Ashkar, A. A. et al. Assessment of requirements for IL-15 and IFN regulatory factors in uterine NK cell differentiation and function during pregnancy. *J. Immunol.* **171**, 2937–2944 (2003).
11. Faas, M. M. & De Vos, P. Innate immune cells in the placental bed in healthy pregnancy and preeclampsia. *Placenta* <https://doi.org/10.1016/j.placenta.2018.04.012> (2018).
12. Karumanchi, S. A., Maynard, S. E., Stillman, I. E., Epstein, F. H. & Sukhatme, V. P. Preeclampsia: a renal perspective. *Kidney Int* **67**, 2101–2113 (2005).
13. Gamliel, M. et al. Trained memory of human uterine NK cells enhances their function in subsequent pregnancies. *Immunity* **48**, 951–962.e955 (2018).
14. Hunkapiller, N. M. et al. A role for Notch signaling in trophoblast endovascular invasion and in the pathogenesis of pre-eclampsia. *Development* **138**, 2987–2998 (2011).
15. Kelly, D., King, T. & Aminov, R. Importance of microbial colonization of the gut in early life to the development of immunity. *Mutat. Res* **622**, 58–69 (2007).
16. Smid, M. C. et al. Maternal gut microbiome biodiversity in pregnancy. *Am. J. Perinatol.* **35**, 24–30 (2018).
17. Holmes, E. et al. Human metabolic phenotype diversity and its association with diet and blood pressure. *Nature* **453**, 396–400 (2008).
18. Schiering, C. et al. Feedback control of AHR signalling regulates intestinal immunity. *Nature* **542**, 242–245 (2017).
19. Yan, Q. et al. Alterations of the Gut Microbiome in Hypertension. *Front Cell Infect. Microbiol* **7**, 381 (2017).
20. Turnbaugh, P. J. et al. The human microbiome project. *Nature* **449**, 804–810 (2007).
21. Patel, S., Preuss, C. V. & Bernice, F. *Vancomycin*. 2024 Oct 29. In: StatPearls [Internet]. Treasure Island (FL): StatPearls Publishing; 2025.
22. Gibbins, K. J. et al. Effects of excess thromboxane A2 on placental development and nutrient transporters in a *Mus musculus* model of fetal growth restriction. *Biol. Reprod.* **98**, 695–704 (2018).
23. Wilson, M. E. & Ford, S. P. Comparative aspects of placental efficiency. *Reprod. Suppl.* **58**, 223–232 (2001).
24. Albers, R. E. et al. Trophoblast-specific expression of Hif-1 α results in Preeclampsia-like symptoms and fetal growth restriction. *Sci. Rep.* **9**, 2742 (2019).
25. Cheng, L., Yu, H., Yan, N., Lai, K. & Xiang, M. Hypoxia-inducible Factor-1 α target genes contribute to retinal neuroprotection. *Front Cell Neurosci.* **11**, 20 (2017).
26. Cheng, S.-B. et al. Pyroptosis is a critical inflammatory pathway in the placenta from early onset preeclampsia and in human trophoblasts exposed to hypoxia and endoplasmic reticulum stressors. *Cell Death Dis.* **10**, 927 (2019).
27. Hussain, T. et al. Understanding the immune system in fetal protection and maternal infections during pregnancy. *J. Immunol. Res* **2022**, 7567708 (2022).
28. Ashkar, A. A., Di Santo, J. P. & Croy, B. A. Interferon gamma contributes to initiation of uterine vascular modification, decidual integrity, and uterine natural killer cell maturation during normal murine pregnancy. *J. Exp. Med* **192**, 259–270 (2000).
29. Chen, Z. et al. DBA-lectin reactivity defines mouse uterine natural killer cell subsets with biased gene expression. *Biol. Reprod.* **87**, 81 (2012).
30. Dunk, C. & Ahmed, A. Expression of VEGF-C and activation of its receptors VEGFR-2 and VEGFR-3 in trophoblast. *Histol. Histopathol.* **16**, 359–375 (2001).
31. Hunter, A. et al. Serum levels of vascular endothelial growth factor in preeclamptic and normotensive pregnancy. *Hypertension* **36**, 965–969 (2000).
32. Ubeda, C. & Pamer, E. G. Antibiotics, microbiota, and immune defense. *Trends Immunol.* **33**, 459–466 (2012).
33. Jiang, W. et al. Dysbiosis gut microbiota associated with inflammation and impaired mucosal immune function in intestine of humans with non-alcoholic fatty liver disease. *Sci. Rep.* **5**, 8096 (2015).
34. Mouries, J. et al. Microbiota-driven gut vascular barrier disruption is a prerequisite for non-alcoholic steatohepatitis development. *J. Hepatol.* <https://doi.org/10.1016/j.jhep.2019.08.005> (2019).
35. Wang, J. et al. Gut microbiota dysbiosis in preeclampsia patients in the second and third trimesters. *Chin. Med J.* **133**, 1057–1065 (2020).
36. Gomez de Agüero, M. et al. The maternal microbiota drives early postnatal innate immune development. *Science* **351**, 1296–1302 (2016).
37. Edlund, C., Barkholt, L., Olsson-Liljequist, B. & Nord, C. E. Effect of vancomycin on intestinal flora of patients who previously received antimicrobial therapy. *Clin. Infect. Dis.* **25**, 729–732 (1997).
38. Derrien, M., Vaughan, E. E., Plugge, C. M. & de Vos, W. M. *Akkermansia muciniphila* gen. nov., sp. nov., a human intestinal mucin-degrading bacterium. *Int J. Syst. Evol. Microbiol* **54**, 1469–1476 (2004).
39. Clapp, J. F. Maternal carbohydrate intake and pregnancy outcome. *Proc. Nutr. Soc.* **61**, 45–50 (2002).
40. Poznanski, S. M. & Ashkar, A. A. What defines NK cell functional fate: phenotype or metabolism? *Front. Immunol.* **10**, 1414 (2019).
41. Donnelly, R. P. et al. mTORC1-dependent metabolic reprogramming is a prerequisite for NK cell effector function. *J. Immunol.* **193**, 4477–4484 (2014).
42. Frey, P. A. The Leloir pathway: a mechanistic imperative for three enzymes to change the stereochemical configuration of a single carbon in galactose. *FASEB J.* **10**, 461–470 (1996).
43. Koren, O. et al. Host remodeling of the gut microbiome and metabolic changes during pregnancy. *Cell* **150**, 470–480 (2012).
44. Hawrelak, J. A. & Myers, S. P. The causes of intestinal dysbiosis: a review. *Alter. Med. Rev.* **9**, 180–197 (2004).
45. Trowsdale, J. & Betz, A. G. Mother's little helpers: mechanisms of maternal-fetal tolerance. *Nat. Immunol.* **7**, 241–246 (2006).
46. Nelson, S. M., Matthews, P. & Poston, L. Maternal metabolism and obesity: modifiable determinants of pregnancy outcome. *Hum. Reprod. Update* **16**, 255–275 (2010).
47. Young, B. C., Levine, R. J. & Karumanchi, S. A. Pathogenesis of preeclampsia. *Annu. Rev. Pathol.* **5**, 173–192 (2010).
48. Zou, H. et al. Changes of gut mycobiota in the third trimester of pregnant women with preeclampsia. *J. Matern.-Fetal Neonatal Med.* **36**, 2228964 (2023).
49. Desforges, M. & Sibley, C. P. Placental nutrient supply and fetal growth. *Int J. Dev. Biol.* **54**, 377–390 (2010).

50. Shenoy, V., Kanasaki, K. & Kalluri, R. Pre-eclampsia: connecting angiogenic and metabolic pathways. *Trends Endocrinol. Metab.* **21**, 529–536 (2010).
51. Murphy, S. P., Fast, L. D., Hanna, N. N. & Sharma, S. Uterine NK cells mediate inflammation-induced fetal demise in IL-10-null mice. *J. Immunol.* **175**, 4084–4090 (2005).
52. Roberts, K. A. et al. Placental structure and inflammation in pregnancies associated with obesity. *Placenta* **32**, 247–254 (2011).
53. Kalkunte, S. S. et al. Vascular endothelial growth factor C facilitates immune tolerance and endovascular activity of human uterine NK cells at the maternal-fetal interface. *J. Immunol.* **182**, 4085–4092 (2009).
54. Dalby, M. J., Ross, A. W., Walker, A. W. & Morgan, P. J. Dietary uncoupling of gut microbiota and energy harvesting from obesity and glucose tolerance in mice. *Cell Rep.* **21**, 1521–1533 (2017).
55. Wu, H. J. & Wu, E. The role of gut microbiota in immune homeostasis and autoimmunity. *Gut microbes* **3**, 4–14 (2012).
56. Cani, P. D. & Delzenne, N. M. The role of the gut microbiota in energy metabolism and metabolic disease. *Curr. Pharm. Des.* **15**, 1546–1558 (2009).
57. Su, Y. et al. Hypothalamic leucine metabolism regulates liver glucose production. *Diabetes* **61**, 85–93 (2012).
58. Arrieta-Cruz, I., Su, Y. & Gutiérrez-Juárez, R. Suppression of endogenous glucose production by isoleucine and valine and impact of diet composition. *Nutrients* **8**, 79 (2016).
59. De Vadder, F. et al. Microbiota-generated metabolites promote metabolic benefits via gut-brain neural circuits. *Cell* **156**, 84–96 (2014).
60. Pugh, S. K. et al. Does hypoglycemia following a glucose challenge test identify a high risk pregnancy? *Reprod. Health* **6**, 10 (2009).
61. Ringholm, L., Nørgaard, S. K., Rytter, A., Damm, P. & Mathiesen, E. R. Dietary advice to support glycaemic control and weight management in women with Type 1 Diabetes during pregnancy and breastfeeding. *Nutrients* **14** <https://doi.org/10.3390/nu14224867> (2022).
62. Furet, J. P. et al. Comparative assessment of human and farm animal faecal microbiota using real-time quantitative PCR. *FEMS Microbiol. Ecol.* **68**, 351–362 (2009).
63. Milani, C. et al. Assessing the fecal microbiota: an optimized ion torrent 16S rRNA gene-based analysis protocol. *PLoS One* **8**, e68739 (2013).
64. Edgar, R. C. Search and clustering orders of magnitude faster than BLAST. *Bioinformatics* **26**, 2460–2461 (2010).
65. Caporaso, J. G. et al. QIIME allows analysis of high-throughput community sequencing data. *Nat. Methods* **7**, 335–336 (2010).
66. Sutcliffe, I. C. A phylum level perspective on bacterial cell envelope architecture. *Trends Microbiol.* **18**, 464–470 (2010).
67. Love, M. I., Huber, W. & Anders, S. Moderated estimation of fold change and dispersion for RNA-seq data with DESeq2. *Genome Biol.* **15**, 550 (2014).
68. Wold, S., Sjöström, M. & Eriksson, L. PLS-regression: a basic tool of chemometrics. *Chemom. Intell. Lab. Syst.* **58**, 109–130 (2001).
69. Sysi-Aho, M., Katajamaa, M., Yetukuri, L. & Oresic, M. Normalization method for metabolomics data using optimal selection of multiple internal standards. *BMC Bioinforma.* **8**, 93 (2007).
70. Mevik, B.-H. & Wehrens, R. The pls Package: Principal Component and Partial Least Squares Regression in R. *J. Stat. Softw.* Vol 1, Issue 2 (2007) (2007).

Acknowledgements

The publication fee for this work was covered by the Italian Ministry of Health's 'Ricerca Corrente' funding to the IRCCS Humanitas Research Hospital. This investigation was financially supported by the Horizon2020, Marie Skłodowska-Curie Individual fellowship 2017 (DaPhNIS 795797-SG).

Author contributions

S.G. designed the study, conceived and performed the experiments, analyzed the data, wrote the manuscript and secured the findings; A.G. analyzed the 16S data and wrote the manuscript, MRusin and S.P. performed experiments and contributed to interpretation of the results. SC and TS provided expertise and feedback. M.C.P. and V.F. performed experiments. MRescigno supervised the study and the findings of the work. All authors discussed the results and contributed to the final version of the manuscript.

Competing interests

The authors declare no competing interests.

Additional information

Supplementary information The online version contains supplementary material available at <https://doi.org/10.1038/s41467-025-58533-8>.

Correspondence and requests for materials should be addressed to Silvia Giugliano or Maria Rescigno.

Peer review information *Nature Communications* thanks Cliona O'Farrelly and the other, anonymous, reviewer(s) for their contribution to the peer review of this work. A peer review file is available.

Reprints and permissions information is available at <http://www.nature.com/reprints>

Publisher's note Springer Nature remains neutral with regard to jurisdictional claims in published maps and institutional affiliations.

Open Access This article is licensed under a Creative Commons Attribution-NonCommercial-NoDerivatives 4.0 International License, which permits any non-commercial use, sharing, distribution and reproduction in any medium or format, as long as you give appropriate credit to the original author(s) and the source, provide a link to the Creative Commons licence, and indicate if you modified the licensed material. You do not have permission under this licence to share adapted material derived from this article or parts of it. The images or other third party material in this article are included in the article's Creative Commons licence, unless indicated otherwise in a credit line to the material. If material is not included in the article's Creative Commons licence and your intended use is not permitted by statutory regulation or exceeds the permitted use, you will need to obtain permission directly from the copyright holder. To view a copy of this licence, visit <http://creativecommons.org/licenses/by-nc-nd/4.0/>.

© The Author(s) 2025